Inorganic Chemistry

Article

pubs.acs.org/IC

Lanthanide-Porphyrin Hybrids: from Layered Structures to Metal–Organic Frameworks with Photophysical Properties

Jan Demel,[†] Pavel Kubát,[‡] Franck Millange,[§] Jérôme Marrot,[§] Ivana Císařová,[∥] and Kamil Lang*[,†]

[†]Institute of Inorganic Chemistry, Academy of Sciences of the Czech Republic, v.v.i., Husinec-Řež 1001, 250 68 Řež, Czech Republic

[‡]J. Heyrovský Institute of Physical Chemistry, Academy of Sciences of the Czech Republic, v.v.i., Dolejškova 3, 182 23 Praha 8, Czech Republic

[§] Institut Lavoisier, UMR CNRS 8180, Université de Versailles Saint-Quentin-en-Yvelines, 45 Avenue des Etats-Unis, 78035 Versailles Cedex, France

[∥]Department of Inorganic Chemistry, Faculty of Science, Charles University in Prague, Hlavova 2030, 128 40 Praha, Czech Republic

Supporting Information

ABSTRACT: Rare-earth layered hydroxides with intercalated tetrasulfonated porphyrins and corresponding to the chemical formula $Ln_2(OH)_{4.7}(Por)_{0.33}\cdot 2H_2O$ (Ln = Eu^{3+}, Tb^{3+}; Por = 5,10,15,20-tetrakis(4-sulfonatophenyl)porphyrin (TPPS) and PdTPPS) have been prepared to investigate their photophysical properties. A slight variation of the synthetic procedure led to the metal–organic framework (MOF) assembled from a distorted octahedral oxometalate clusters $[Eu_6(\mu_6\text{-}O)(\mu_3\text{-}OH)_8(H_2O)_{14}]^{8+}$. These secondary building units (SBUs) are linked together by six distorted porphyrin units. During activation, the original SBU loses not only water molecules from the coordination sphere but also the central μ_6-O atom. The loss of the central atom results in the distortion of the octahedral $[Eu_6(\mu_6\text{-}O)(\mu_3\text{-}OH)_8(H_2O)_{14}]^{8+}$ SBU into a trigonal antiprismatic $[Eu_6(\mu_3\text{-}OH)_8(H_2O)_2]^{10+}$ SBU with two μ_3-OH groups nearly in plane with the europium atoms and the reduction of pores to approximately 2 × 3 Å. As a result, the MOF has no accessible porosity. This transformation was thoroughly characterized by means of single-crystal X-ray crystallographic analysis of both phases. Solid-state photophysical investigations suggest that the MOF material is fluorescent; however, in contrast to the prepared layered hydroxides, the as-prepared MOF is an effective sensitizer of singlet oxygen, $O_2(^1\Delta_g)$, with a relatively long lifetime of 23 ± 1 μs. The transition is also accompanied by variation in photophysical properties of the coordinated TPPS. The alteration of the fluorescence properties and of the $O_2(^1\Delta_g)$ lifetime presents an opportunity for preparation of MOFs with oxygen-sensing ability or with oxidation potential toward organic molecules by $O_2(^1\Delta_g)$.

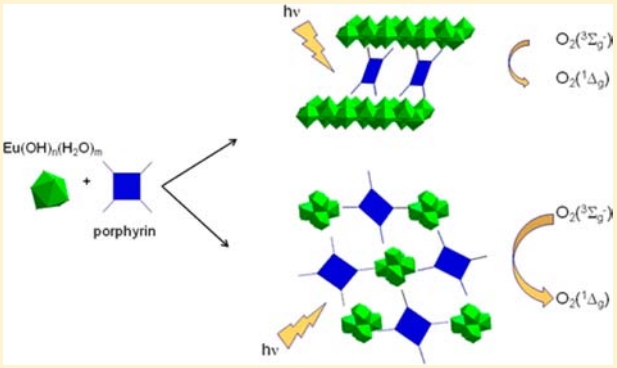

INTRODUCTION

Inorganic–organic hybrid materials have great potential for a variety of applications.[1,2] In particular, the utilization of layered hydroxides in the design of novel materials has emerged in applications relating to light absorption, sensing, magnetism, delivery systems, and photosensitization.[3−5] The structure of layered hydroxides consists of positively charged, stacked hydroxide layers with anionic species in the interlayer spacing. The anion-exchange properties of these materials enable easy modification and fine-tuning of the derived properties. Extensive research has been performed on layered double hydroxides (LDHs) with the general formula $[M^{2+}_{1-x}M^{3+}_x(OH)_2A^{n-}_{x/n}]\cdot mH_2O$, where M^{2+} and M^{3+} are, respectively, divalent and trivalent cations arranged in brucite-like hydroxide layers, and A represents the anionic species. Growing interest has been directed toward layered simple hydroxides (LSHs) with the layers composed of a single type of metal cations and the positive charge imposed by hydroxyl vacancies.[3,6] The hydroxide layer structure of LSHs varies, for example, $Cu_2(OH)_3(A^-)\cdot H_2O$ and $Ni_2(OH)_3(A^-)\cdot H_2O$ contain the hydroxide layers composed of octahedrally coordinated cations, whereas $Zn_5(OH)_8(A^-)_2\cdot 2H_2O$ and $Co_2(OH)_3(A^-)\cdot H_2O$ exhibit a three-layer arrangement with octahedrally and tetrahedrally coordinated metal cations.

Recently, a series of layered rare-earth hydroxides (LRHs) with the general composition $Ln_2(OH)_5(A^-)\cdot xH_2O$ and $Ln_2(OH)_4(A^-)_2\cdot 1.5H_2O$ have been synthesized because of increased research interest in their unique ability to combine the properties of lanthanide ions with the host–guest chemistry of LDHs.[7−9] The lanthanide luminescence properties, their structural variability, and the tunable hydroxide composition make LRHs an intriguing group of materials. In addition, the synthesis conditions can be controlled[10,11] to obtain either two-

Received: January 24, 2013
Published: February 20, 2013

   dx.doi.org/10.1021/ic400182u | Inorg. Chem. 2013, 52, 2779–2786

dimensional (2D) layered hydroxides or three-dimensional (3D) metal−organic frameworks (MOFs), which combine the light emission property of rare-earth metals with the porosity of a MOF structure.[12,13] The permanent porosity of several luminescent MOFs has enabled the reversible storage and release of guest substrates, thus providing the host with specific abilities.

Porphyrins are structurally functional robust molecules with relatively rigid geometry and terminal functional groups that can be easily varied; such characteristic properties make porphyrins an ideal class of building blocks for the synthesis of crystalline MOFs.[14−16] A variety of porphyrin-based MOFs directed by the coordination bonding between organic struts and metal nodes and their resulting coordination geometries have been documented in the literature. Despite the fact that the research on porphyrinic MOFs is in its initial stage,[17,18] some MOFs demostrate promise for potential applications in catalysis,[19−21] photocatalysis,[22] and gas separation and storage because of their ability to preferentially adsorb oxygen[23] and weakly interacting gas molecules.[24] Porphyrinic MOFs also show promise in the design of thermoresponsive,[25] electrochemical,[26] light-harvesting,[27] and luminescent devices.[28]

Herein we report on the preparation of europium and terbium layered hydroxides intercalated with 5,10,15,20-tetrakis(4-sulfonatophenyl)porphyrin (TPPS) and Pd(II)-5,10,15,20-tetrakis(4-sulfonatophenyl)porphyrin (PdTPPS). Variations in the synthesis procedure changed the product of the reaction from a 2D layered structure to a MOF structure composed of hexanuclear oxometalate clusters with interconnecting TPPS units. The structure of the MOF in the as-prepared and activated forms, the luminescent properties of the porphyrin molecules affected by the bonding within the crystal structure, and the ability of the porphyrins to produce singlet oxygen have been described.

EXPERIMENTAL SECTION

Materials. The TPPS dihydrochloride, PdTPPS tetrasodium salt, (both from Frontier Scientific Europe, Ltd., U.K.), $Eu(NO_3)_3{\cdot}6H_2O$, $Tb(NO_3)_3{\cdot}6H_2O$ (both from Strem Chemicals), and NaOH (Penta, Czech Republic) were used as purchased.

Synthesis of Layered Hydroxides Intercalated with Porphyrins. The materials were prepared by precipitation followed by hydrothermal treatment analogous to the procedure reported by McIntyre et al.[9] In a typical experiment, 0.0625 mmol of porphyrin was dissolved in 20 mL of deionized water followed by the addition of 0.1 M NaOH: 8.0 mL (0.8 mmol) or 11.1 mL (1.1 mmol) for the PdTPPS- or TPPS-containing materials, respectively (higher amounts of NaOH were used to convert TPPS to the tetrasodium salt). Following this step, 0.5 mmol of Eu or Tb nitrate dissolved in water was added under stirring. The final pH of the solutions was in the range of 6.5−6.8. The mixture was stirred for 15 min at room temperature (RT) and then transferred into a PTFE-lined stainless steel autoclave (Berkhoff) and inserted into a 150 °C preheated oven for 48 h. After cooling to RT, the products were filtered through an S4 frit, washed with water and acetone, and air-dried at RT. In all cases, the reaction yielded 120−130 mg of deep purple (TPPS) or red (PdTPPS) powder.

Synthesis of MOFs. For a typical synthesis, 0.5 mmol of $Eu(NO_3)_3{\cdot}6H_2O$ was added to a 0.0625 stirred solution of TPPS·2HCl in 20 mL of deionized water. The dark green solution turned into a light green suspension that was stirred for 5 min; then 5.55 mL of 0.1 M NaOH was added over the course of 30 min to yield the final pH value of 6.5−7.0. The suspension was then stirred for 15 min, transferred into a PTFE-lined stainless steel autoclave (Berkhoff), and heated at 150 °C for 48 h. The resulting mixture of small platelet-like particles of layered europium hydroxide (LEuH-TPPS) and crystals (needles) of the as-prepared MOF-Eu-TPPS was separated by decantation followed by washing with water. The reaction yielded approximately 50 mg of deep purple crystals. The procedure and its variations did not yield MOF-Eu-PdTPPS or Tb^{3+}-based MOFs.

Instrumental Methods. Powder X-ray diffraction (XRD) patterns were recorded on a PANalytical X'Pert PRO diffractometer operating in the transmission mode. In this setup, the incident Cu X-ray beam (40 kV, 30 mA) passed through an elliptical focusing mirror, 0.5°divergence slit, 0.5° antiscatter slit, and a 0.02 rad Soller slit. A fast linear position sensitive detector PIXcel with an antiscatter shield and a 0.02 rad Soller slit were used for the diffracted beam. All patterns were collected in the range between 1 and 88° (2θ) with a step of 0.0065° (510 s/step). Qualitative analysis was performed with the HighScorePlus software package (PANalytical, Almelo, The Netherlands, version 3.0) and the JCPDS PDF-2 database.[29]

In situ high-temperature XRD measurements (HT-XRD) were performed in an Anton Paar HTK16 high-temperature chamber with a PANalytical X'Pert PRO diffractometer (CoKα radiation, X'Celerator multichannel detector) in air. Powder samples were gently ground with the addition of few drops of water and deposited on a Pt-plate using a micropipet to form a thin layer upon drying. The Pt-plate served as both a sample holder and heating medium. A heating program was used to control the heating and cooling processes (both with a step of 10 °C, heating/cooling rate of 2 °C min^{-1}) and set a delay time of 24 h between the heating/cooling cycles.

Fourier-transform infrared spectra (FTIR) were recorded using a Nicolet NEXUS 670-FT spectrometer and KBr pellets. Absorption spectra were collected on a Perkin-Elmer Lambda 35 spectrometer equipped with a Labsphere RSA-PE-20 integration sphere. The samples were diluted with $BaSO_4$. The spectra were converted from reflection to absorbance by the Kubelka−Munk method. Thermal analyses (TG/DTA/MS) were carried out on a Setaram SETSYS Evolution-16-MS instrument coupled with a mass-spectrometry system. The measurements were performed in synthetic air atmosphere (flow rate 30 mL min^{-1}) from 30 to 1000 °C with a heating rate of 5 °C min^{-1}.

The luminescence properties were monitored on a Fluorolog 3 spectrometer equipped with a cooled TBX-05-C photon detection module (Horiba Jobin Yvon) or with a Hamamatsu H10330-45 photomultiplier for measurement of the $O_2(^1\Delta_g)$ emission spectra. The powders were placed in a holder that was oriented 30° to the excitation source. The TPPS fluorescence lifetime measurements were performed using a laser-diode excitation at 405 nm (NanoLED-405LH, pulse width 750 ps, repetition rate 1 MHz). The emission was recorded at both fluorescence maxima using a cooled TBX-05-C photon detection module in a time-correlated single-photon counting regime. The decay curves were fitted to exponential functions using the iterative reconvolution procedure of the DAS6 software (v. 6.4, Horiba Jobin Yvon, 2009).

The time-resolved near-infrared luminescence of $O_2(^1\Delta_g)$ at 1270 nm was monitored using a Ge detector upon laser excitation by a Lambda Physik Compex 102 excimer laser (λ_{exc} = 308 nm, pulse width 28 ns, incident energy 2−4 mJ/pulse). The short-lived signal produced by the scattering of an excitation laser pulse and/or by porphyrin fluorescence was eliminated by exciting the sample in vacuum and subtracting the obtained signal from the signal recorded in oxygen or air atmosphere. The signal-to-noise ratio was improved by averaging 100 to 500 individual traces.

Crystal Structure Determination. A single black crystal of as-prepared MOF-Eu-TPPS was mounted onto a Lindemann capillary and measured using a Bruker APEX-II CCD diffractometer with monochromatized MoKα radiation (λ = 0.71073 Å) at 150 K. A numerical absorption was applied (μ = 3.14 mm^{-1}, T_{min} = 0.469, T_{max} = 0.720) and a total of 101603 measured reflections were collected in the range h = −46 to 61, k = −14 to 14, l = −36 to 36 (θ_{max} = 27.5°), out of which 14496 were unique (R_{int} = 0.044) and 11985 were observed according to the $I > 2\sigma(I)$ criterion. Cell parameters were calculated from 9753 reflections (θ = 2.9−27.5°). The structure was solved by direct methods (SHELXS) and refined using the full-matrix least-squares based on F^2 (SHELXL97).[30,31] Hydrogen atoms were

dx.doi.org/10.1021/ic400182u | Inorg. Chem. 2013, 52, 2779−2786

fixed into idealized positions (riding model) and assigned temperature factors $H_{iso}(H) = 1.2U_{eq}$ (pivot atom). The refinement converged ($\Delta/\sigma_{max} = 0.006$) to $R = 0.030$ for the observed reflections and $wR(F^2) = 0.072$, GOF = 0.99 for 710 parameters and all 14496 reflections. The final difference map displayed no significant chemical peaks ($\Delta\rho_{max} = 1.33$, $\Delta\rho_{min} = -0.59$ e Å^{-3}). Voids forming channels around the *b*-axis were filled with disordered water molecules. As the position of these water molecules could not be resolved on the Fourier maps, PLATON/SQUEEZE was used to compensate the data for their contribution to the diffraction patterns. Eight potential solvent volumes ranging from 330 to 450 Å^3 were found in the unit cell, and 1128 electrons per unit cell worth of scattering were located in the voids with the highest peak, corresponding to an electron density of 8.9 e Å^{-3}. The SQUEEZE procedure resulted in a reasonably precise solvent-free model that converged at $R = 0.030$ (from 0.069 before correction), enabling location of the hydrogen atoms in the porphyrin moiety.

A black crystal of dehydrated MOF-Eu-TPPS was mounted onto a cryoloop via the viscous oil-drop method. X-ray intensity data were collected on a Bruker X8-APEX-II CCD diffractometer by monochromatized MoKα radiation at 200 K. A numerical absorption was applied ($\mu = 3.64$ mm^{-1}, $T_{min} = 0.561$, $T_{max} = 0.868$), and a total of 22413 measured reflections in the range $h = -54$ to 54, $k = -10$ to 10, $l = -33$ to 37 ($\theta_{max} = 25.1°$), of which 9559 were unique ($R_{int} = 0.040$), and 7497 were observed according to the $I > 2\sigma(I)$ criterion. Unit cell parameters were calculated from 6102 reflections ($\theta = 2.3-25.1°$), and the structure was solved by direct methods (SHELXS) and refined by full-matrix least-squares based on F^2 (SHELXL97).[30,31] Hydrogen atoms were fixed into idealized positions (riding model) and assigned temperature factors $H_{iso}(H) = 1.2U_{eq}$ (pivot atom). The refinement converged ($\Delta/\sigma_{max} = 0.001$) to $R = 0.045$ for the observed reflections and $wR(F^2) = 0.128$, GOF = 1.16 for 652 parameters and all 9559 reflections. The final difference map displayed no chemically significant peaks.

The crystallographic data are summarized in Table 1 and in the Supporting Information. The crystallographic material can also be obtained from the CCDC, the deposition numbers are CCDC 894308 and 894309.

Table 1. Crystalographic Data for the Monoclinic MOF-Eu-TPPS

	MOF-Eu-TPPS	
	as-prepared	dehydrated
empirical formula	$C_{88}H_{88}Eu_6N_8O_{47}S_8$	$C_{88}H_{64}Eu_6N_8O_{34}S_8$
formula weight/g mol^{-1}	3177.9	2945.7
T/K	150(2)	200(2)
crystal system	monoclinic	monoclinic
space group	$C2/c$ (no. 15)	$C2/c$ (no. 15)
a/Å	47.1489(12)	45.950(2)
b/Å	10.9944(3)	9.1496(5)
c/Å	28.3561(8)	31.3267(15)
β/deg	120.563(1)	124.211(1)
cell volume/Å^3	12656.93(61)	10891.6(9)
Z	4	4
calc. density/g cm^{-3}	1.668	1.796
abs. coefficient/mm^{-1}	3.142	3.635
θ range for data collection/deg	2.85−27.5	1.07−25.11
cryst. size/mm^3	0.11 × 0.19 × 0.28	0.04 × 0.12 × 0.18
independent reflections	14496	9559
data/restraint/parameters	14496/0/710	7497/0/652
goodness-of-fit on F^2	0.99	1.16
wR_2 (all data)	0.072	0.128
R_1 (all data)	0.042	0.067
$\Delta\rho_{min}$/ $\Delta\rho_{max}$/e Å^{-3}	−0.59/1.33	−1.42/1.17

RESULTS AND DISCUSSION

Preparation and Characterization of LRHs. The layered europium and terbium hydroxides intercalated with TPPS and PdTPPS, hereafter abbreviated as LEuH-TPPS, LEuH-PdTPPS, LTbH-TPPS, and LTbH-PdTPPS, were prepared by precipitation followed by hydrothermal treatment.[9] The combination of powder XRD, elemental analysis, FTIR, and TG/DTA/MS confirmed the layered structure of the materials with the charge-compensating porphyrin anions in the interlayer spacing. The composition is consistent with the chemical formula $Ln_2(OH)_{4.7}(TPPS)_{0.33}\cdot 2H_2O$ (see the Supporting Information, Table S1).

The powder XRD patterns of the prepared materials are shown in Figure 1. A series of 00*l* diffractions are characteristic

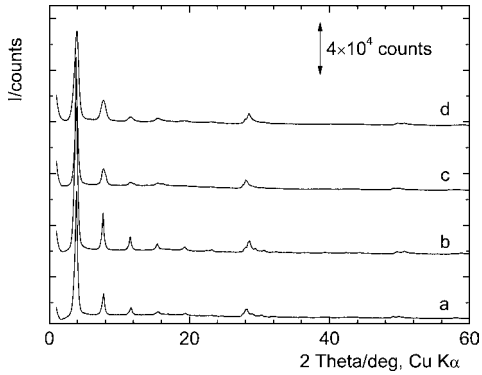

Figure 1. Powder XRD pattern of LEuH-TPPS (a), LTbH-TPPS (b), LEuH-PdTPPS (c), and LTbH-PdTPPS (d). The curves are vertically shifted for better clarity.

of a layered phase and correspond to a basal spacing of 22.4−23.3 Å, thus confirming that the LRH structure is intercalated with bulky organic anions.[10,32,33] The basal spacing is similar to the values previously reported for LDHs (21.7−23.0 Å)[34] or layered zinc hydroxide (approximately 22−23 Å)[35] intercalated with sulfonated porphyrin anions. The high affinity of the anionic porphyrins toward the hydroxide layers is indicated by the fact that all basal diffraction lines can be assigned to pure phases. In addition, all prepared samples have a number of weak nonbasal diffractions in the regions 27−30°, 48.5−50°, and 56.5−60° (2θ), indicating that the structure and composition of the hydroxide layers are preserved after porphyrin intercalation.

The TG/DTA/MS data display three distinct mass losses comparable to those observed for other layered hydroxides (Supporting Information, Figures S1−S4). The first mass loss step occurs below 130 °C and corresponds to a loss of 2−3 water molecules that are mostly co-intercalated with porphyrin anions in the interlayer spacing. A second mass loss is noted by the dehydration of the hydroxide layers, and it is associated with the release of water molecules; this process is completed below 300 °C. The intercalated porphyrin molecules decompose at approximately 400 °C, as shown by the CO_2, NO_2, SO_2, and H_2O gas release. Porphyrinic sulfur is the main component released above 700 °C as SO_2 and is most likely derived from thermally stable mixed rare-earth oxide sulfates formed during the heating, as analogously reported for porphyrin-layered zinc hydroxide hybrids.[36] The total mass loss corresponds to the conversion of the original materials to the oxide Ln_2O_3. All FTIR spectra are highly similar and display

dx.doi.org/10.1021/ic400182u | Inorg. Chem. 2013, 52, 2779−2786

peaks belonging to the TPPS or PdTPPS vibrations (Supporting Information, Figure S5). The sulfonate antisymmetric and symmetric vibrations within the ranges of 1174−1169 and 1038−1039 cm^{-1}, respectively, are in good agreement with those of TPPS and PdTPPS intercalated in layered zinc hydroxide or LDH hosts.[35]

Preparation and Characterization of MOF-Eu-TPPS. As indicated in the experimental section, a slight variation of the procedure, namely, neutralization of the $Eu(NO_3)_3$ and TPPS solutions by the addition of 0.1 M NaOH, led to a different acid−base behavior. In this case, a final pH value of 6.5−7.0 was achieved using half of the amount of NaOH typically required in the synthesis of the LRH-porphyrin hybrids. The product, as-prepared MOF-Eu-TPPS, was always accompanied by the LEuH-TPPS phase that was removed by repeated sedimentation. Attempts to prepare MOFs with terbium and MOF-Eu-PdTPPS yielded crystals of very poor quality that quickly disintegrated. The higher ionic radius of Tb^{3+} and the forced planarity of the porphyrin moiety introduced by Pd in PdTPPS are evidently parameters that are not compatible with the stable crystal structure of MOF-Eu-TPPS as described below.

Good agreement between the measured powder XRD and the simulated pattern obtained from the single-crystal X-ray crystallographic analysis (see below) reveals the high purity of the material (Supporting Information, Figure S6). The identity of MOF-Eu-TPPS was complemented by the elemental (Supporting Information, Table S1) and thermal analysis that documents the loss of 26 water molecules between 30 and 229 °C (Supporting Information, Figures S7). The porphyrin moiety decomposes at approximately 340 and 490 °C, as was the case for the LRH hybrids, and the decomposition observed above 800 °C is related to the release of sulfur. The FTIR spectrum is dominated by the TPPS vibrations (Supporting Information, Figure S5); the symmetric sulfonate vibration at 1038 cm^{-1} is comparable to that of the LRH hybrids, whereas the antisymmetric band is slightly shifted to 1163 cm^{-1} as a result of the four coordination modes of the sulfonate groups (see below).

HT-XRD of as-prepared MOF-Eu-TPPS revealed a change between 60 and 100 °C that was ascribed to the loss of structural water (Figure 2). In agreement with the thermal analysis, the sample appears to be chemically stable up to 200 °C. No immediate structural change indicated by powder XRD occurs upon cooling the sample to room temperature; however, when the sample is left in ambient conditions for 1 h, the original XRD patterns of as-prepared MOF-Eu-TPPS reappear because of rehydration of the activated material through ambient humidity. The dehydration−rehydration process can be reversed, as presented in Figure 2, at the expense of sample crystallinity and of the reappearance rate of the original structure (the rate considerably decreases after the fourth cycle, and more than 24 h is needed for full conversion to the as-prepared structure). The powder XRD patterns of the dehydrated form are in good agreement with the simulated patterns obtained from the single-crystal X-ray crystallographic study (see below) (Supporting Information, Figure S8). As revealed from adsorption studies, the activated form of MOF-Eu-TPPS has no accessible porosity for nitrogen or krypton.

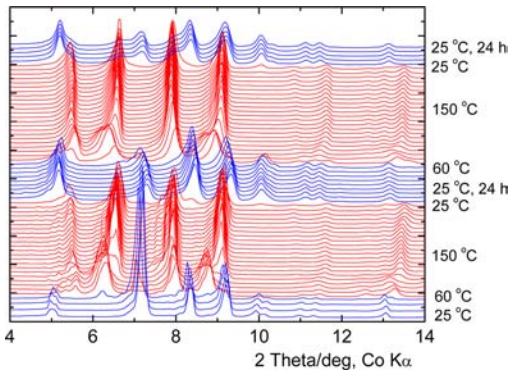

Figure 2. HT-XRD of as-prepared MOF-Eu-TPPS during heating/cooling cycles in air. The sample was heated from 25 to 150 °C, followed by cooling back to 25 °C. The next cycle was performed after 24 h. For better clarity, the XRD patterns from 25 to 60 °C are shown in blue.

Crystal Structure of As-Prepared MOF-Eu-TPPS. Full crystallographic details are given in Table 1. The structure is composed of distorted octahedral oxometalate clusters $[Eu_6(\mu_6\text{-}O)(\mu_3\text{-}OH)_8(H_2O)_{14}]^{8+}$. This SBU unit is linked together by six distorted porphyrin units (Figure 3a). The central oxygen atom is coordinated to six europium atoms that are also connected via eight OH groups located above the center of each face (Figure 4).

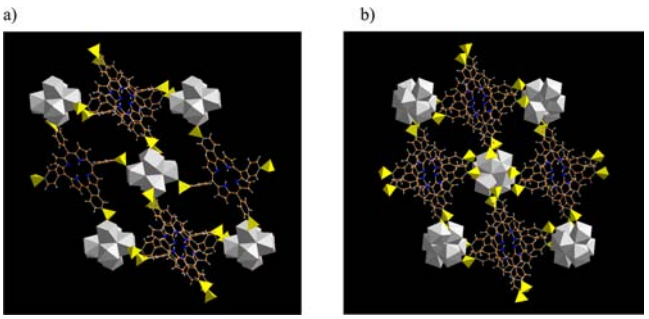

Figure 3. Polyhedral view of the structure of as-prepared MOF-Eu-TPPS (a) and its dehydrated form (b) along the *b*-axis. Europium polyhedra are white and sulfonate tetrahedra are yellow; elements are color-coded as follows: N (blue), C (orange), and H (white).

Three independent europium sites are found in this structure. Although all europium sites are nine coordinate and surrounded by four μ_3-OH groups and the central μ_6-O, they are distinct in the number of coordinated water molecules and the coordination mode of the sulfonate groups to the europium centers. The coordination sphere of Eu1 is completed by one terminal water molecule and three oxygen atoms coming from two different sulfonate groups (two oxygen atoms from the same sulfonate group acting as a bidentate chelating ligand and one oxygen atom of another sulfonate group acting as a bridge between Eu1 and Eu2). Three terminal water molecules therefore complete the nine coordination sphere of Eu2. Finally, Eu3 is connected to one oxygen atom of a sulfonate group (monodentate chelating mode) and three terminal water molecules. For comparison, $[Ln_6(\mu_6\text{-}O)(\mu_3\text{-}OH)_8(NO_3)_6(H_2O)_n]^{2+}$ is a similar SBU coordinated with nitrate anions[37−39] that can be partially replaced by terephthalic acid to form a 1D coordination polymer,[40] or SBUs can be joined by *p*-sulfonatocalix[4]arene, leading to a MOF structure.[41] Considering the porphyrin side, the TPPS linker is connected to three SBUs via the sulfonate groups (Figure 4). Interestingly, the three interacting sulfonate groups of each TPPS differ in their coordination mode; they vary from

dx.doi.org/10.1021/ic400182u | Inorg. Chem. 2013, 52, 2779−2786

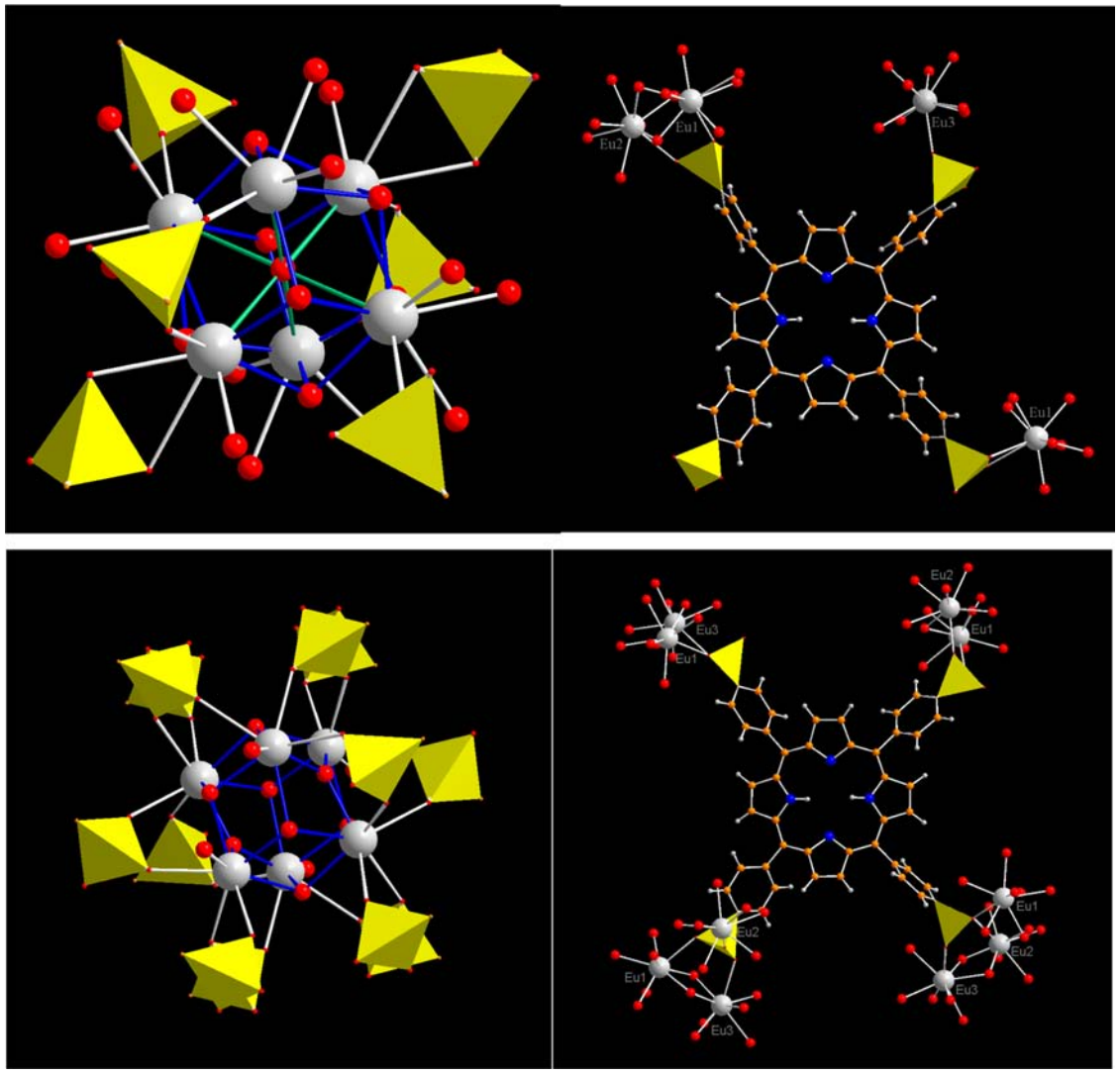

Figure 4. View of the structural change upon dehydration: SBU (left) and TPPS (right) units for the as-prepared (top) and dehydrated (bottom) MOF-Eu-TPPS structures. For better clarity, the sulfonated tetrahedra are shown in yellow; elements are color-coded as follows: N (blue), C (orange), O (red), H (small white), Eu (large white).

monodentate and bidentate mononuclear coordination (chelating) to bidentate binuclear coordination (bridging). This intriguing feature results in the tilted stacking of the porphyrin units along the *b*-axis, most likely favored by $\pi-\pi$ interactions. The porphyrin units exhibit a nonplanar saddle deformation with the displacement of the pyrrole rings alternatively above and below the mean porphyrin plane and the *meso* carbon atoms approximately within the plane (Supporting Information, Figure S10). These nonplanar deformations are typical for porphyrins with overcrowded periphery by many moderately bulky groups or several bulky substituents.[42] In the present case, the porphyrin unit is not stabilized by a central metal that makes the unit easily distorted by packing bulky SBUs. The interplanar distance between planes created by the *meso* carbon atoms of the TPPS units is approximately 3.8 Å. The linking of SBUs by TPPS forms pores of approximately ~4 × 5 Å along the *b*-axis filled with 12 molecules of water per unit. As a result, the volume accessible to the solvent represents approximately 25% of the cell volume (Supporting Information, Figure S9).

Crystal Structure of Dehydrated MOF-Eu-TPPS. Full crystallographic details for the dehydrated MOF-Eu-TPPS are also listed in Table 1. The dehydrated MOF-Eu-TPPS shows the same space group as the as-prepared material; however, the shrinking of the void volume leads to the decrease of the cell volume by approximately 1765 Å^3 (Supporting Information, Figure S9). In fact, the *a* and *b* parameters decrease, whereas the *c* parameter increases during the dehydration process. Interestingly, the original oxometalate $[Eu_6(\mu_6\text{-}O)(\mu_3\text{-}OH)_8(H_2O)_{14}]^{8+}$ cluster loses not only water molecules from the coordination sphere but also the central μ_6-O atom. This change causes the distortion of the octahedral $[Eu_6(\mu_6\text{-}O)(\mu_3\text{-}OH)_8(H_2O)_{14}]^{8+}$ SBU into a trigonal antiprismatic $[Eu_6(\mu_3\text{-}OH)_8(H_2O)_2]^{10+}$ SBU with two μ_3-OH groups nearly in plane with the europium atoms (Figure 4). It should be noted that four terminal water molecules with partial occupancy (50%) were found in the cluster. The presence of the terminal water molecules is attributed to partial rehydration that occurred during the selection and mounting of the crystal on a goniometer head. The structure is built up from a trigonal antiprismatic SBU $[Eu_6(\mu_3\text{-}OH)_8(H_2O)_2]^{10+}$ (Figure 3b), in which 6 europium atoms bridged by the μ_3-OH groups connect with 12 sulfonate groups from 12 different porphyrin units. The coordination numbers of the three nonequivalent Eu atoms in SBU of the dehydrated phase decrease from nine to eight (or

dx.doi.org/10.1021/ic400182u | *Inorg. Chem.* 2013, 52, 2779−2786

seven depending on the partial presence of the coordinated water molecules to two europium sites); four of the coordination positions are occupied by OH groups, and the rest are filled by the oxygen atoms of the porphyrin sulfonate groups. This behavior is in contrast to what is observed for complexes with the general formula $[Ln_6(\mu_6\text{-}O)(\mu_3\text{-}OH)_8(NO_3)_6(H_2O)_x]^{2+}$ (x = 12 for Ln = Sm–Yb, x = 14 for Ln = Pr–Nd, x = 16 for Ln = Ce).[37] These complexes dehydrate to polymeric chains with the chemical formula $[Ln_6(\mu_6\text{-}O)(\mu_3\text{-}OH)_8(NO_3)_8]$ without the loss of the central μ_6-O atoms and with more condensed packing of the oxometalate clusters. From the porphyrin side, the TPPS linker is connected to four SBUs via the sulfonate groups (Figure 4). Interestingly, the interacting sulfonate groups of each TPPS differ in their coordination mode from bidentate binuclear coordination (bridging) to monodentate mononuclear coordination (chelating).

The Eu–Eu distance is prolonged from 3.57–3.69 Å to 3.70–3.82 Å between Eu atoms at the base of the trigonal antiprism, and to 3.86–3.90 Å between Eu atoms occupying the side faces. For comparison, the porphyrin units in the dehydrated phase are more planar and are closer to each other (3.65 compared with 3.8 Å). The pores are reduced to approximately 2 × 3 Å along the *b*-axis, leading to no accessible porosity.

Absorption Spectra. The absorption spectra of the porphyrins can be used to observe the formation of specific porphyrin aggregates within the interlayer spacing or adsorbed onto crystal surfaces of the LRHs.[4,43] The mutual arrangement of the stacked porphyrin units can be categorized into one of two types: (i) J-aggregates (edge-to-edge) are characterized by a red shift of the porphyrin Soret band, whereas (ii) H-aggregates (face-to-face) exhibit a blue shift of the porphyrin Soret band. In general, the aggregation considerably decreases the quantum yields of the excited states because of the fast vibrational relaxation of the excited aggregates that is manifested by overall low photoactivity.

The absorption spectra of LEuH-TPPS and LTbH-TPPS are characterized by the Soret band at 416 nm and four Q-bands at 518, 550, 592, and 648 nm (Figure 5). Evidently, the intercalation of TPPS broadens the Soret band when compared with the sharp Soret band of the monomeric species in an aqueous solution.[44] The observed spectral features exclude the presence of the specific stacked structures of TPPS molecules within the interlayer spacing and can be attributed to strong interactions between the periphery of individual molecules and the densely packed hydroxide layers through a range of different orientations of the porphyrin molecules relative to each other and with respect to the hydroxide layers.[4] The results are similar to those reported for LDHs intercalated with TPPS.[34,44] The absorption spectra of intercalated PdTPPS in LEuH-PdTPPS and LTbH-PdTPPS are very similar to each other. The Soret band at 413 nm is slightly broadened when compared with PdTPPS aqueous solutions, and the Q(1,0) band is red-shifted from 520 to 527 nm. Similar to TPPS, no specific aggregates of PdTPPS within the interlayer spacing of the LRHs are detected.

The absorption spectrum of as-prepared MOF-Eu-TPPS differs from those of LEuH-TPPS and LTbH-TPPS. The Soret band is split into two bands with maxima at 416 and approximately 450 nm, and the Q-bands are red-shifted to 528, 563, 601, and 655 nm. The spectral changes of individual molecules have been correlated with the degree of porphyrin deformation.[42,45] As demonstrated by the spectra, free-base porphyrins with a nonplanar macrocycle because of steric crowding of peripheral substituents have Soret band maxima shifted up toward 450 nm when compared with the planar free-base porphyrin used as a reference. The increase in the degree of nonplanarity is also accompanied by red shifts of the Q-bands and by the increase of relative intensity of the lowest energy $Q_x(0,0)$ band with respect to the other Q-bands. All of these features can be observed in the case of the as-prepared MOF-Eu-TPPS and are in accord with the single-crystal X-ray analysis indicating the saddle deformation of the linking porphyrin units (see above).

Photofunctions of Intercalated Porphyrins. Nitrate layered hydroxide $Eu_2(OH)_5NO_3$ has typical Eu^{3+} emission lines at 579, 589–595, 615, 653, and 698 nm when excited in the UV region, similar to the emission described by Zhu et al.[46] In contrast, all of the prepared LRH hybrids exhibit only luminescence properties imposed by the intercalated porphyrins because of their strong absorption at wavelengths used for the excitation of Eu^{3+}. The fluorescence emission spectra of LEuH-TPPS and LTbH-TPPS have Q(0,0) and Q(0,1) emission bands at 660 and 716 nm, respectively (Figure 6). The bands are red-shifted when compared with TPPS in aqueous solution (642 and 703 nm) and with TPPS

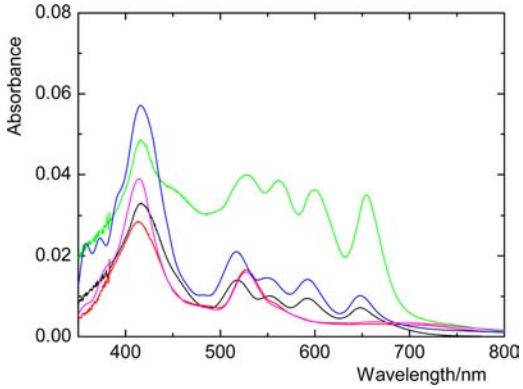

Figure 5. UV/vis absorption spectra of solid LEuH-TPPS (blue), LTbH-TPPS (black), LEuH-PdTPPS (magenta), LTbH-PdTPPS (red), and as-prepared MOF-Eu-TPPS (green).

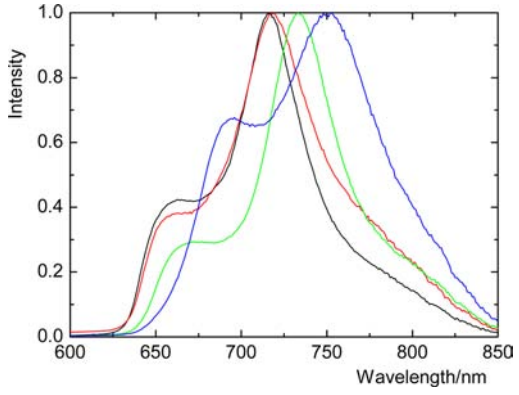

Figure 6. Normalized fluorescence emission spectra of TPPS in solid LEuH-TPPS (black), LTbH-TPPS (red), as-prepared MOF-Eu-TPPS (green), and dehydrated MOF-Eu-TPPS (blue). Solid samples were excited at 420 nm.

dx.doi.org/10.1021/ic400182u | Inorg. Chem. 2013, 52, 2779–2786

intercalated in Mg_2Al LDHs (649 and 716 nm).[44] The obtained results reveal that TPPS molecules in the interlayer spacing remain photoactive; however, intercalated TPPS molecules more intimately interact with the LRH hydroxide layers than with the LDH hydroxide layers. The enhanced interaction is also documented by the considerably increased Q(0,1) emission band over the Q(0,0) band and by fast fluorescence decays that are best characterized by two lifetimes: 0.6 (86%) and 2.5 ns (14%). The luminescence spectra of LEuH-PdTPPS and LTbH-PdTPPS exhibit both fluorescence (614 nm) and phosphorescence emission bands (~ 715 and 780 nm) (Supporting Information, Figure S11). The strong interactions of the PdTPPS units with the hydroxide layers are, similarly to those of TPPS, evidenced by a large red shift of all of the emission bands when compared with the corresponding bands of PdTPPS in aqueous solution (606, 700, and 765 nm) and the interlayer spacing of Mg_2Al LDH (607, 687, and 760 nm).[44] In summary, the described emission properties reflect the coordination interactions of the porphyrins with the LRH layers and packing of the porphyrin units in the interlayer spacing.

The appearance of an emission at 1270 nm indicated the formation of $O_2(^1\Delta_g)$ upon excitation of LEuH-TPPS in an oxygen atmosphere. The observed lifetime of approximately 4 μs is very short and demonstrates that the fate of $O_2(^1\Delta_g)$ within the layered host is controlled by the decay of the parental triplet states. In the case of intercalated PdTPPS, the $O_2(^1\Delta_g)$ signals were not observed, most likely because they were obscured by the scattering of an excitation laser pulse and/or by porphyrin luminescence. These results are in agreement with the short intrinsic lifetime of $O_2(^1\Delta_g)$ in LDH matrixes and highlight the key effects of the OH groups coordinated to the metal centers of the hydroxide layers and the water molecules confined in the interlayer spacing on the quenching of $O_2(^1\Delta_g)$.[4]

Effect of the Transformation of MOF-Eu-TPPS on Photophysical Properties. The fluorescence emission spectrum of the solid as-prepared MOF-Eu-TPPS has emission bands at approximately 670 and 733 nm (Figure 6) that are red-shifted when compared with those of LEuH-TPPS. The Q(0,1) band also has a higher relative intensity than the Q(0,0) band at 670 nm. The fluorescence decays have similar lifetimes of 0.9 (66%) and 2.4 ns (34%) when compared to the intercalated TPPS in LEuH-TPPS, with a slightly increased contribution of the long-lived component. Evidently, the fluorescence features are related to the packing of the TPPS units and the porphyrin-porphyrin interactions, as the average distance between the porphyrin units in the crystal structure of as-prepared MOF-Eu-TPPS is approximately 3.8 Å, which is similar for porphyrin aggregates. In accord with the increasing porphyrin-porphyrin interactions within the structure of dehydrated MOF-Eu-TPPS (the distance between TPPS units is 3.65 Å), the fluorescence emission bands are significantly red-shifted to 695 and 750 nm (Figure 6), and the fluorescence lifetimes decrease to 0.4 (81%) and 1.9 ns (19%).

In contrast to LEuH-TPPS, an intense $O_2(^1\Delta_g)$ luminescence was observed after excitation of the solid as-prepared MOF-Eu-TPPS, making this material the first reported MOF that produces $O_2(^1\Delta_g)$ (Figure 7). A relatively long $O_2(^1\Delta_g)$ lifetime of 23 ± 1 μs was observed in both air and oxygen, indicating that the fate of $O_2(^1\Delta_g)$ is much less governed by the decay of the TPPS triplet states, as was the case for LEuH-TPPS, and that the as-prepared MOF-Eu-TPPS can act as a sensitizer of

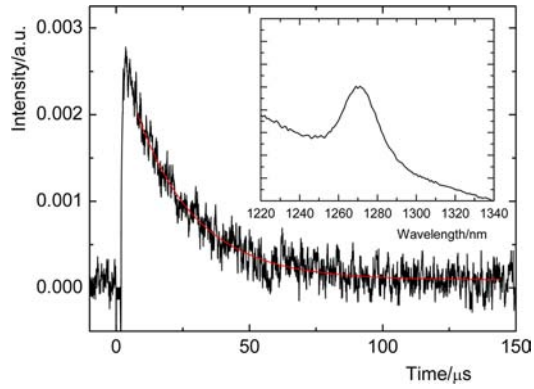

Figure 7. Relaxation of the $O_2(^1\Delta_g)$ luminescence signal produced by 308 nm excitation of solid as-prepared MOF-Eu-TPPS in air (black line). The red line is a least-squares monoexponential fit. Inset: Emission band of $O_2(^1\Delta_g)$ obtained upon excitation of the solid at 520 nm.

$O_2(^1\Delta_g)$ for photooxidation processes. Dehydrated MOF-Eu-TPPS exhibits a slightly decreased $O_2(^1\Delta_g)$ lifetime of 16 ± 1 μs. The shorter lifetime can be related to the interactions of $O_2(^1\Delta_g)$ within the MOF structure and/or to the partial quenching of the porphyrin triplet states because of the more closely packed porphyrin units.

CONCLUSIONS

We have used tetrasulfonated porphyrins and europium or terbium cations to construct novel hybrid materials whose photophysical properties are governed by the arrangement of the porphyrin units within the structure. We have also demonstrated that the appropriate control of reaction conditions can successfully lead to the synthesis of rare-earth layered hydroxides with intercalated porphyrins within the hydroxide layers or to the incorporation of the porphyrin units into the MOF possessing the features needed for effective photofunctional materials. The structure of the MOF is composed of $[Eu_6(\mu_6\text{-}O)(\mu_3\text{-}OH)_8(H_2O)_{14}]^{8+}$ SBUs that are linked together by distorted porphyrin units and can be transformed into trigonal antiprismatic $[Eu_6(\mu_3\text{-}OH)_8(H_2O)_2]^{10+}$ SBUs after activation. Both MOF phases were characterized in detail with single-crystal X-ray crystallographic analysis. The capability of the MOF to produce long-lived $O_2(^1\Delta_g)$ in comparison to the LRHs with the intercalated porphyrins gives impetus to the design of novel multifunctional porphyrinic MOFs with tuned photoresponses and porosity and that have perspective sensing, bactericidal, and photooxidative properties. Additionally, the MOF presents interesting framework-dependent fluorescent properties that are sensitive to the alignment of the porphyrin units. We are currently investigating the syntheses of porphyrinic MOFs with porosity.

ASSOCIATED CONTENT

Supporting Information

Full experimental details (elemental analysis, characterization, XRD data, structural description, luminescence, CIF files). This material is available free of charge via the Internet at http://pubs.acs.org.

AUTHOR INFORMATION

Corresponding Author

*E-mail: lang@iic.cas.cz.

Notes

The authors declare no competing financial interest.

■ ACKNOWLEDGMENTS

This work was supported by the Czech Science Foundation (P207/10/1447). We are grateful to Petr Bezdička (IIC, ASCR, Řež) for performing powder XRD measurements.

■ REFERENCES

(1) Férey, G. *Chem. Soc. Rev.* **2008**, *37*, 191−214.
(2) Sanchez, C.; Rozes, L.; Ribot, F.; Laberty-Robert, C.; Grosso, D.; Sassoye, C.; Boissiere, C.; Nicole, L. *C. R. Chim.* **2010**, *13*, 3−39.
(3) Rogez, G.; Massobrio, C.; Rabu, P.; Drillon, M. *Chem. Soc. Rev.* **2011**, *40*, 1031−1058.
(4) Demel, J.; Lang, K. *Eur. J. Inorg. Chem.* **2012**, 5154−5164.
(5) Yan, D.; Lu, J.; Wei, M.; Evans, D. G.; Duan, X. *J. Mater. Chem.* **2011**, *21*, 13128−13139.
(6) Arizaga, G. G. C.; Satyanarayana, K. G.; Wypych, F. *Solid State Ionics* **2007**, *178*, 1143−1162.
(7) Geng, F.; Ma, R.; Sasaki, T. *Acc. Chem. Res.* **2010**, *43*, 1177−1185.
(8) McIntyre, L. J.; Prior, T. J.; Fogg, A. M. *Chem. Mater.* **2010**, *22*, 2635−2645.
(9) McIntyre, L. J.; Jackson, L. K.; Fogg, A. M. *Chem. Mater.* **2008**, *20*, 335−340.
(10) Gándara, F.; Puebla, E. G.; Iglesias, M.; Proserpio, D. M.; Snejko, N.; Monge, M. Á. *Chem. Mater.* **2009**, *21*, 655−661.
(11) Goulding, H. V.; Hulse, S. E.; Clegg, W.; Harrington, R. W.; Playford, H. Y.; Walton, R. I.; Fogg, A. M. *J. Am. Chem. Soc.* **2010**, *132*, 13618−13620.
(12) Cui, Y.; Yue, Y.; Qian, G.; Chen, B. *Chem. Rev.* **2012**, *112*, 1126−1162.
(13) Rocha, J.; Carlos, L. D.; Paz, F. A. A.; Ananias, D. *Chem. Soc. Rev.* **2011**, *40*, 926−940.
(14) Zou, C.; Wu, C.-D. *Dalton Trans.* **2012**, *41*, 3879−3888.
(15) Burnett, B. J.; Barron, P. M.; Choe, W. *CrystEngComm* **2012**, *14*, 3839−3846.
(16) Goldberg, I. *Chem. Commun.* **2005**, 1243−1254.
(17) Lipstman, S.; Muniappan, S.; George, S.; Goldberg, I. *Dalton Trans.* **2007**, 3273−3281.
(18) Smythe, N. C.; Butler, D. P.; Moore, C. E.; McGowan, W. R.; Rheingold, A. L.; Beauvais, L. G. *Dalton Trans.* **2012**, *41*, 7855−7858.
(19) Shultz, A. M.; Farha, O. K.; Hupp, J. T.; Nguyen, S. T. *J. Am. Chem. Soc.* **2009**, *131*, 4204−4205.
(20) Farha, O. K.; Shultz, A. M.; Sarjeant, A. A.; Nguyen, S. T.; Hupp, J. T. *J. Am. Chem. Soc.* **2011**, *133*, 5652−5655.
(21) Morris, W.; Volosskiy, B.; Demir, S.; Gándara, F.; McGrier, P. L.; Furukawa, H.; Cascio, D.; Stoddart, J. F.; Yaghi, O. M. *Inorg. Chem.* **2012**, *51*, 6443−6445.
(22) Xie, M.-H.; Yang, X.-L.; Zou, C.; Wu, C.-D. *Inorg. Chem.* **2011**, *50*, 5318−5320.
(23) Fateeva, A.; Devautour-Vinot, S.; Heymans, N.; Devic, T.; Grenèche, J.-M.; Wuttke, S.; Miller, S.; Lago, A.; Serre, C.; De Weireld, G.; Maurin, G.; Vimont, A.; Férey, G. *Chem. Mater.* **2011**, *23*, 4641−4651.
(24) Chen, W.-T.; Yamada, Y.; Liu, G.-N.; Kubota, A.; Ichikawa, T.; Kojima, Y.; Guo, G.-C.; Fukuzumi, S. *Dalton Trans.* **2011**, *40*, 12826−12831.
(25) DeVries, L. D.; Barron, P. M.; Hurley, E. P.; Hu, C.; Choe, W. *J. Am. Chem. Soc.* **2011**, *133*, 14848−14851.
(26) Jahan, M.; Bao, Q.; Loh, K. P. *J. Am. Chem. Soc.* **2012**, *134*, 6707−6713.
(27) Zou, C.; Xie, M.-H.; Kong, G.-Q.; Wu, C.-D. *CrystEngComm* **2012**, *14*, 4850−4856.
(28) Lee, C. Y.; Farha, O. K.; Hong, B. J.; Sarjeant, A. A.; Nguyen, S. T.; Hupp, J. T. *J. Am. Chem. Soc.* **2011**, *133*, 15858−15861.
(29) JCPDS PDF-2 database, International Centre for Diffraction Data, Newtown Square, PA, U.S.A. release 54, 2004.
(30) Altomare, A.; Cascarano, G.; Giacovazzo, C.; Guagliardi, A.; Burla, M. C.; Polidori, G.; Camalli, M. *J. Appl. Crystallogr.* **1994**, *27*, 435−435.
(31) Sheldrick, G. M. *SHELXL97*; University of Göttingen: Göttingen, Germany, 1997.
(32) Yoon, Y.-S.; Lee, B.-I.; Lee, K. S.; Im, G. H.; Byeon, S.-H.; Lee, J. H.; Lee, I. S. *Adv. Funct. Mater.* **2009**, *19*, 3375−3380.
(33) Hu, L.; Ma, R.; Ozawa, T. C.; Geng, F.; Iyi, N.; Sasaki, T. *Chem. Commun.* **2008**, 4897−4899.
(34) Káfuňková, E.; Taviot-Guého, C.; Bezdička, P.; Klementová, M.; Kovář, P.; Kubát, P.; Mosinger, J.; Pospíšil, M.; Lang, K. *Chem. Mater.* **2010**, *22*, 2481−2490.
(35) Demel, J.; Kubát, P.; Jirka, I.; Kovář, P.; Pospíšil, M.; Lang, K. *J. Phys. Chem. C* **2010**, *114*, 16321−16328.
(36) Demel, J.; Pleštil, J.; Bezdička, P.; Janda, P.; Klementová, M.; Lang, K. *J. Colloid Interface Sci.* **2011**, *360*, 532−539.
(37) Calvez, G.; Daiguebonne, C.; Guillou, O.; Pott, T.; Méléard, P.; Le Dret, F. *C. R. Chim.* **2010**, *13*, 715−730.
(38) Žák, Z.; Unfried, P.; Giester, G. *J. Alloys Compd.* **1994**, *205*, 235−242.
(39) Giester, G.; Unfried, P.; Žák, Z. *J. Alloys Compd.* **1997**, *257*, 175−181.
(40) Calvez, G.; Daiguebonne, C.; Guillou, O. *Inorg. Chem.* **2011**, *50*, 2851−2858.
(41) Gándara, F.; Gutiérrez-Puebla, E.; Iglesias, M.; Snejko, N.; Monge, M. Á. *Cryst. Growth Des.* **2010**, *10*, 128−134.
(42) Senge, M. O. *Chem. Commun.* **2006**, 243−256.
(43) Kubát, P.; Lang, K.; Procházková, K.; Anzenbacher, P. *Langmuir* **2003**, *19*, 422−428.
(44) Jiřičková, M.; Demel, J.; Kubát, P.; Hostomský, J.; Kovanda, F.; Lang, K. *J. Phys. Chem. C* **2011**, *115*, 21700−21706.
(45) Sazanovich, I. V.; Galievsky, V. A.; van Hoek, A.; Schaafsma, T. J.; Malinovskii, V. L.; Holten, D.; Chirvony, V. S. *J. Phys. Chem. B* **2001**, *105*, 7818−7829.
(46) Zhu, Q.; Li, J.-G.; Zhi, C.; Li, X.; Sun, X.; Sakka, Y.; Golberg, D.; Bando, Y. *Chem. Mater.* **2010**, *22*, 4204−4213.